Excited state spectroscopy of the silica sol–gel glass activated by Cr^{5+} and Cr^{6+} ions

2002 J. Phys.: Condens. Matter 14 11553

(http://iopscience.iop.org/0953-8984/14/45/301)

INSTITUTE OF PHYSICS PUBLISHING JOURNAL OF PHYSICS: CONDENSED MATTER

J. Phys.: Condens. Matter **14** (2002) 11553–11572 PII: S0953-8984(02)37710-5

Excited state spectroscopy of the silica sol–gel glass activated by Cr^{5+} and Cr^{6+} ions

Cz Koepke[1], **K Wiśniewski**[1], **M Grinberg**[2] **and F Rozpłoch**[1]

[1] Institute of Physics, N Copernicus University, Grudziądzka 5/7, 87-100 Toruń, Poland
[2] Institute of Experimental Physics, University of Gdańsk, Wita Stwosza 57, 80-952 Gdańsk, Poland

Received 6 June 2002
Published 1 November 2002
Online at stacks.iop.org/JPhysCM/14/11553

Abstract

We report on the optical spectroscopy of the silica sol–gel glass doped with chromium of various valences where Cr^{6+} and Cr^{5+} ions appear to be most active. The presence of the Cr^{5+} ions in six-fold coordination is seen in the luminescence spectra and decays whereas the Cr^{6+} ions in four-fold coordination are mostly responsible for the excited state absorption (ESA), but also give a contribution to the luminescence. We interpret the ESA in terms of transitions between crystal field split terms of the $Cr^{5+}O^{-}$ centre which forms after the charge transfer (CT) transition, and between one of those terms and another, double-electron state of larger electron–lattice coupling, which forms after two consecutive transitions of electrons via the CT transition. The luminescence and decay characteristics are due to the composition of the transitions in both Cr^{5+} and $Cr^{5+}O^{-}$ centres, the former interpreted in terms of the Jahn–Teller effect in the d^1 system in the octahedral coordination, along with the nuances associated with that effect; the latter ones being the triplet–singlet or singlet–singlet transitions depending on temperature.

(Some figures in this article are in colour only in the electronic version)

1. Introduction

Silica sol–gel glasses are attractive as possible laser hosts mostly because of the relatively simple and cheap method of growing them. There are a number of reports on glasses doped with chromium, which is the most popular transition metal dopant (e.g. [1–5]). Although chromium ions have a natural tendency to situate in sites preferring trivalent states (especially in octahedral coordination, as in ruby, alexandrite or garnets), in silica sol–gel glasses the situation is more complex. As shown in [5], in these hosts chromium can occur in several different valences simultaneously. The oxidation reactions during hydrolysis and dealcoholation seem to follow

the routes:

$$4Cr^{3+} + O_2 \rightarrow 4Cr^{4+} + 2O^{2-}$$
$$2Cr^{3+} + O_2 \rightarrow 2Cr^{5+} + 2O^{2-}$$
$$4Cr^{3+} + 3O_2 \rightarrow 4Cr^{6+} + 6O^{2-}$$

where the second route occurs with maximum probability [5]. Indeed, all the aforementioned valences in various centres are seen in the optical properties of chromium doped sol–gel glasses. In this paper we focus our attention only on Cr^{6+} and Cr^{5+} ions because the features of Cr^{4+} are seen only in the absorption spectrum and the possible luminescence connected with their excitation is not seen up to 1300 nm.

Although there are several reports on the luminescence characteristics in this type of material (e.g. [5–8]), only one of them [8] gives a comprehensive interpretation of the optical properties of the material under excitation. In [8] the authors interpret the luminescence of the Cr:silica sol–gel glass in terms of the four-fold-coordinated Cr^{5+} ions (luminescence around $\sim$1.5 μm) and the Cr^{6+} ions coupled to Cr^{5+} (luminescence around 655 nm). In this paper, though describing a very similar material and grown by the same source, we give an alternative interpretation, analysing the absorption and excitation spectra, luminescence spectra, luminescence decays, EPR spectra and the excited state absorption (ESA) spectra.

2. Experimental details

The material has been prepared using the method described in detail in [5]. The samples originated from another series than those examined in [8], hence they can differ a little in structure. More specifically, our samples did not reveal thermoluminescence of the type described in [8], and any luminescence in the IR region (no trace of the luminescence going from that peaking at $\sim$710 nm to IR up to 1300 nm). Such a luminescence has been ascribed to the Cr^{5+} ions in tetrahedral sites in [8]. Analysis of the ionic radii done in [8] shows that the substitutions of the Cr^{5+} ions into tetrahedral and octahedral sites are equally probable. Hence we believe that the samples used in [8] were grown in conditions preferring Cr^{5+} in the tetrahedral sites whereas ours were grown in conditions preferring Cr^{5+} in the octahedral sites. We have examined the samples of different chromium concentration, yellowish with lower concentration and greenish with higher, both of the order of $\sim$0.03 mol%.

Measurements of the absorption spectra, emission spectra and decays were performed independently, in various equipment, to make sure that the obtained characteristics are true. The absorption and emission spectra were measured with an AVIV 14DS spectrometer (slits: 0.5 mm) and a 0.5 m grating monochromator and photomultiplier (Hamamatsu R928), respectively, and also using a liquid-nitrogen-cooled germanium detector (North Coast Optics) and lock-in amplification in the emission case. The decays were measured by a PMT coupled to a SR430 photon counter. The luminescence excitation spectra were registered by a Perkin–Elmer LS50B luminescence spectrometer. The ESA spectrum has been measured using two alternative set-ups. One of them was similar to that described in [9] utilizing a CW source of excitation (Ar ion laser), CW tungsten lamp as a source of probe beam and a chopper lock-in technique and 0.4 m grating monochromator + PMT in the detection branch. The second set-up utilized a RD-EXC-150/25 XeCl excimer laser (308 nm) as a source of excitation, a Hamamatsu Xe flash lamp as a source of probe beam and an ORIEL InstaSpec II photodiode array detector coupled to a MultiSpec 1/8 m spectrograph in the detection branch. The first ESA set-up worked in the CW regime and longitudinal geometry of beams passing through the sample, and the second in the pulsed regime and transverse geometry. The EPR spectra have been measured with a Bruker B-ER-418SM spectrometer.

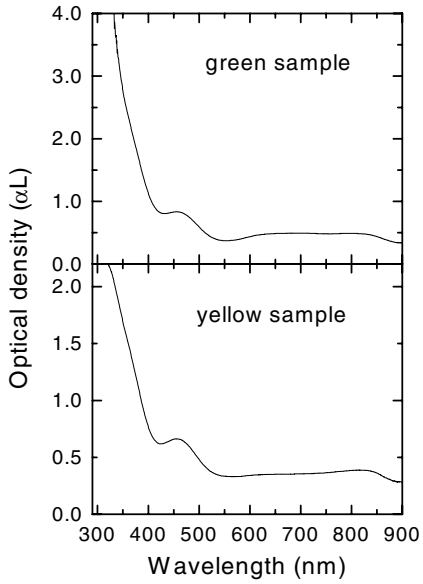

Figure 1. GSA spectra of the green and yellow sample.

3. Results

Ground state absorption (GSA) spectra for two sol–gel samples of green and yellow colour are illustrated in figure 1. The weak and broad band, situated around 700 nm and spreading from 600 to 900 nm, can be assigned to transitions within the Cr^{4+} ion (e.g. [3]) which, we believe, even if emitting in the IR, does not interfere with the reported processes. Following Herren *et al* [6] and Yuan *et al* [10] we can preliminarily assign the peak around 470 nm to intra-ion transition within the Cr^{5+} ions in six-fold coordination ($^2T_{2g} \rightarrow {}^2E_g$ transition). The higher energy shoulder (∼360 nm), being a weak peak immersed in the lattice absorption band, can be attributed to the Cr^{6+} in four-fold coordination. Under excitation into the 360 nm peak the following charge transfer (CT) occurs in the framework of the $[CrO_4]^{2-}$ group [10, 11]:

$$Cr^{6+}O^{2-}(3d^02p^6) \rightarrow Cr^{5+}O^{-}(3d^12p^5).$$

As is shown later in this paper, such a CT absorption has two maxima [4, 11]: the aforementioned lower energy maximum, around 360–370 nm, and a higher energy peak around 270 nm [4]. We cannot see the higher CT peak because of extremely large host absorption in the region of its occurrence.

According to [12] and [13] the tetrahedrally coordinated Cr^{4+} ions should manifest also in the CT onset for energies higher than 40 000 cm^{-1}. Such an onset, if it exists, is entirely immersed in the band-to-band absorption of the glass matrix. Because we cannot directly excite the material into energies sufficiently high for this CT transition we can ignore the influence of these CT states on our observations.

The luminescence spectra of the green sol–gel sample measured by photomultiplier and cooled germanium photodetector, as described in the caption, at low temperature (LT) (∼10 K) and room temperature (RT) for the excitation wavelength 457.9 nm are shown in figure 2. The yellow samples reveal practically identical spectra and the only small differences in the luminescence are in decay profiles, which shall be discussed later. In general the spectra are broad and rather structureless, apart from two features seen at LT for higher photon energies,

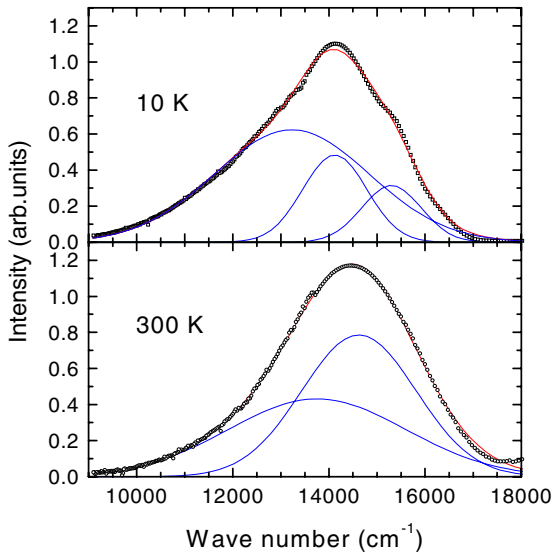

Figure 2. Low- and room-temperature emission spectra for the 457.9 nm excitation.

especially when fitting with Gaussians. These features can find interpretation after analysis of the luminescence excitation spectra presented in figure 3 for the green and yellow sample. Looking at these spectra, monitored at 600 nm, we can see at least three dominant bands (approximated by Gaussians on the energy scale). In comparison with the GSA spectra there is a new distinct feature: a predominant band situated between two bands of ∼470 nm (∼21 000–21 400 cm^{-1}) and ∼360 nm (∼27 500–27 700 cm^{-1}) seen already in the GSA spectra (figure 4), namely large band peaking at ∼400 nm (∼25 000 cm^{-1}). The origin of this as well as the 470 nm band is the Jahn–Teller (JT) effect, which can be seen after detailed analysis of the emission spectra, luminescence decay profiles and EPR spectrum. The highest energy band as placed exactly at the energy ∼27 600–27 800 cm^{-1} (∼360 nm) can be ascribed to the lower maximum of the aforementioned CT absorption in Cr^{6+} ions, whereas the high energy sloped characteristic in the GSA spectrum can be attributed to the lattice states forming a conduction band. As seen in figure 4 the GSA spectra can be easily fitted by Gaussian bands peaking exactly at the same photon energies as the bands forming the excitation spectra.

The typical decay profiles measured at LT and RT are presented in figure 5. The detailed analysis of these decays is given in section 5. At first sight a multiexponential character of all the decays can be noted: such a multiexponential decay is characteristic for the glasses that are systems of a large site-to-site disorder [14, 15]. There are also distinct fast and slow components at LT whereas at RT one cannot distinguish such components.

As supplementary investigations into the time-integrated emission spectra and the luminescence decay measurements we have performed measurements of the time-resolved emission (TRE) spectra. The emission spectra of both samples measured at RT appear to decay identically. Therefore in figure 6 we present the exemplary TRE spectra for the yellow sample detected at 117, 217 and 517 ns. The spectra were fitted by two Gaussians. The first observation is a shift of the maximum to the higher energies with rising time. It is connected with the faster decay of the lower-energy component of the spectrum. It is interesting that at RT we can see here a residual behaviour similar to that at LT, namely the fast component at lower photon energies and the slower one at higher energies. After 517 ns the spectrum decays

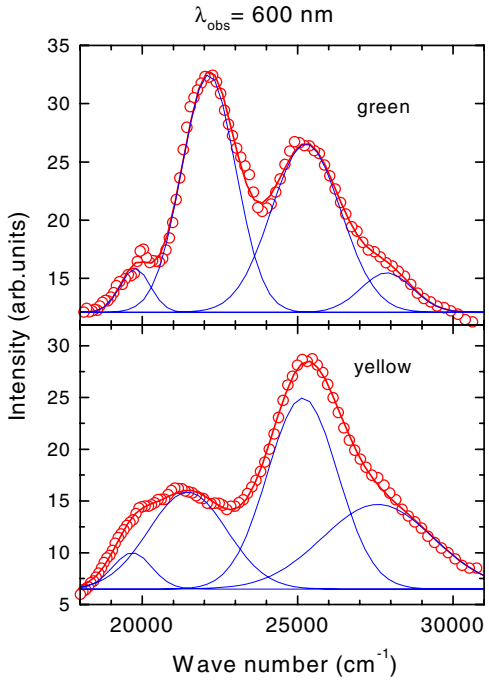

Figure 3. Luminescence excitation spectra monitored at $\lambda = 600$ nm.

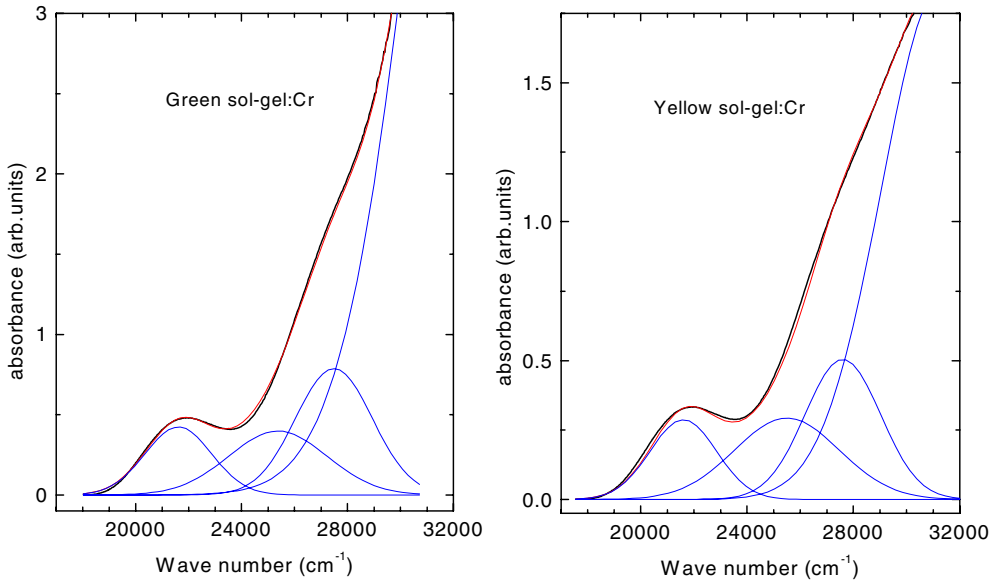

Figure 4. GSA spectra decomposed into Gaussians.

gradually with a characteristic time of the order of several microseconds, keeping more or less the same shape.

In section 5 we try to combine these results with the decay analysis.

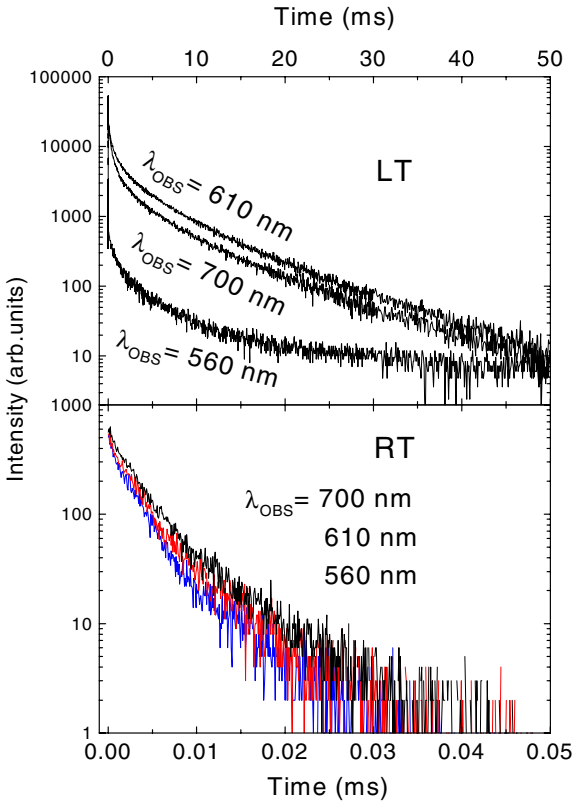

Figure 5. Typical low-(10 K) and RT decay profiles.

Our first and preliminary ESA measurements performed with a very simple CCD array system (Ocean Optics S-1000 spectrometer) were briefly reported in [5]. The present measurements were performed with much more sensitive equipment of better resolution (InstaSpec II + MultiSpec 1/8 by ORIEL). The ESA spectra measured by the pulsed technique with 308 nm excitation are illustrated in figure 6. The spectra depicted are free from the influence of the GSA bleaching [5, 16] that allows us to interpret the ESA spectra directly. The two well defined bands are seen in these spectra. Their interpretation in terms of the transitions in the framework of the d^0-type complex and CT transition in the $[CrO_4]^{2-}$ group is described in section 7.

4. Absorption, emission, luminescence excitation spectra and luminescence decay

As seen in figures 3 and 4 there are at least three absorption bands that, when excited, are responsible for the measured luminescence characteristics. We believe that they are connected with the Cr^{5+} ions in the octahedral coordination [6, 10] and with the Cr^{6+} ions in the tetrahedral coordination [10, 11].

The Cr^{5+} ions in octahedral coordination are the 'handbook type' systems of the d^1 configuration, virtually identical to the Ti^{3+} [17–19] and V^{4+} systems [20]. In such systems the JT effect manifests in a distinct splitting of the ground and terminal GSA state ($^2T_{2g}$ and ^2E_g, respectively) that results from the electron–lattice coupling of the T and E terms to the two-

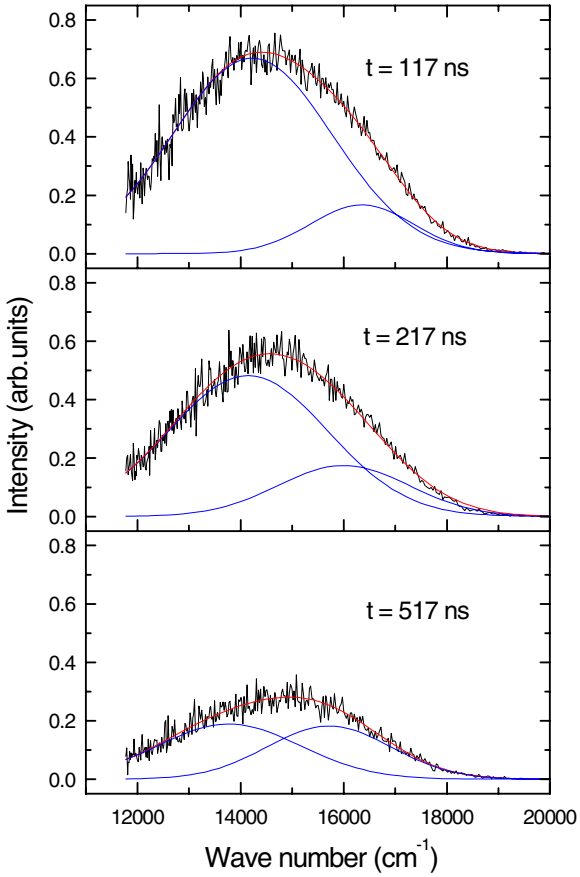

Figure 6. TRE spectra detected at RT.

dimensional vibrational mode ϵ_g. In particular, the ^2E_g electronic manifold (excited state), as a result of the $^2E_g \otimes \epsilon_g$ coupling, in such a situation takes a so-called Mexican hat [21, 22] form. Hence, the two absorption bands (seen first of all in the excitation spectra) of Cr^{5+} ions should be ascribed to the JT split ^2E_g state [20, 22, 23]. The third band, peaking around 360 nm ($\sim$27 700 cm^{-1}), can most likely be ascribed to the CT transition in the frame of the Cr^{6+} ions. The fact that we can see this feature in the luminescence excitation spectrum, monitored at different wavelengths, proves that either there is some energy transfer from the excited $[CrO_4]^{2-}$ group to the Cr^{5+} ions, or that the excited $[CrO_4]^{2-}$ group is also responsible for the emission. On the other hand, the emission spectrum measured at RT is rather structureless and broad (exactly the same situation occurs in Ti^{3+} or V^{4+} systems), looking at first sight like originating from one type of site (with a possible influence of the site-to-site disorder, like in the glasses). This may look unusual in view of the JT splitting of the ground term $^2T_{2g}$. However, at RT the emission probability from the bottom trough of the Mexican hat-like hypersurface to the ground state is the same, regardless of the current position in the trough of the ^2E_g state. Because of the different splitting and positions of the manifolds constituting the $^2T_{2g}$ state seen from the trough of the ^2E_g state (as a result of the $^2T_{2g} \otimes \epsilon_g$ coupling the $^2T_{2g}$ state forms actually three intersecting paraboloids, the system not being cylindrically symmetric, like the ^2E_g state), the transitions from the ^2E_g state end up in the rich variety of the $^2T_{2g}$ state

energies. Such an averaging of the transition energies causes the structureless luminescence spectrum. This dynamic situation is well described in the classic article of Sturge [20] and is well recognized in the case of the spectrum of the Ti^{3+}:Al_2O_3 and Ti–sapphire lasers [24, 25]. The above description concerns the band peaking at RT at $\sim$14 500 cm^{-1}. The remaining band, peaking at RT at $\sim$13 500 cm^{-1}, is most likely to be connected with the $Cr^{5+}O^-$ centre of $\sim T_d$ symmetry.

Other evidence of the JT effect is seen in the LT emission spectra where the characteristic features occur at 14 100 and 15 350 nm. The simple Mexican hat-like shape of the split ^2E_g manifold corresponds to the assumption of harmonic vibrations. It becomes more complex when the admixture of anharmonic vibrations is taken into account, which seems to be closer to the real situation. In such a case an actual shape of the Mexican hat transforms to that having three local valleys (wells) in the bottom trough and appropriate barriers (saddles) between them [21, 22]. The number of valleys depends on the number of symmetry axes and existence of the inversion invariance of the JT vibrational mode. As shown in [22] in the case of octahedral symmetry there are three wells and three saddles placed symmetrically around the central symmetry axis of the Mexican hat. At LT the population is frozen in the wells and only from these points can the transitions occur to the ground state (three intersecting paraboloids of the $^2T_{2g}$ manifold, but only two are accessible for transitions from a given well). Because the wells are situated in equivalent positions with respect to the $^2T_{2g}$ manifold this would favour transitions to two well defined and equivalent points of the $^2T_{2g}$ hypersurface. Hence also appropriate features should be seen at LT. Indeed, looking at LT luminescence spectra one can see at least two weak peaks superimposed on the broad spectrum. Those peaks disappear at RT, which is consistent with the above description (the depth of the wells is $\leqslant$200 cm^{-1}).

5. Luminescence decay analysis

5.1. Observations

The exemplary decays measured at various wavelengths and low and room temperature are illustrated in figure 5. For detailed analysis we assumed that the luminescence originates in the variety of sites that, excited, contribute independently to the emission. In view of the site-to-site disorder in glasses such an assumption is quite natural [14, 15]. Hence the total emission is a superposition of the luminescence from a number of sites and therefore it is not single-exponential, although each site is characterized by single-exponential luminescence decay. In glasses one can assume that the sites are characterized by continuous distribution of the decay constants given by the function $A(\tau)$. Thus the luminescence decay can be expressed by

$$I(t) = \int \frac{A(\tau)}{\tau} e^{-t/\tau}\, d\tau. \tag{1}$$

To recover the distribution $A(\tau)$ from the experimental luminescence decay one should minimize the χ^2 function defined as

$$\chi^2 = \sum_k \frac{\{I_{ex}(t_k) - I(t_k)\}^2}{\sigma_k^2} \tag{2}$$

where $I_{ex}(t_k)$ is the experimental emission intensity at the time t_k, $I(t_k)$ is the calculated intensity according to (1) and σ_k is the weighting of the experimental point, k.

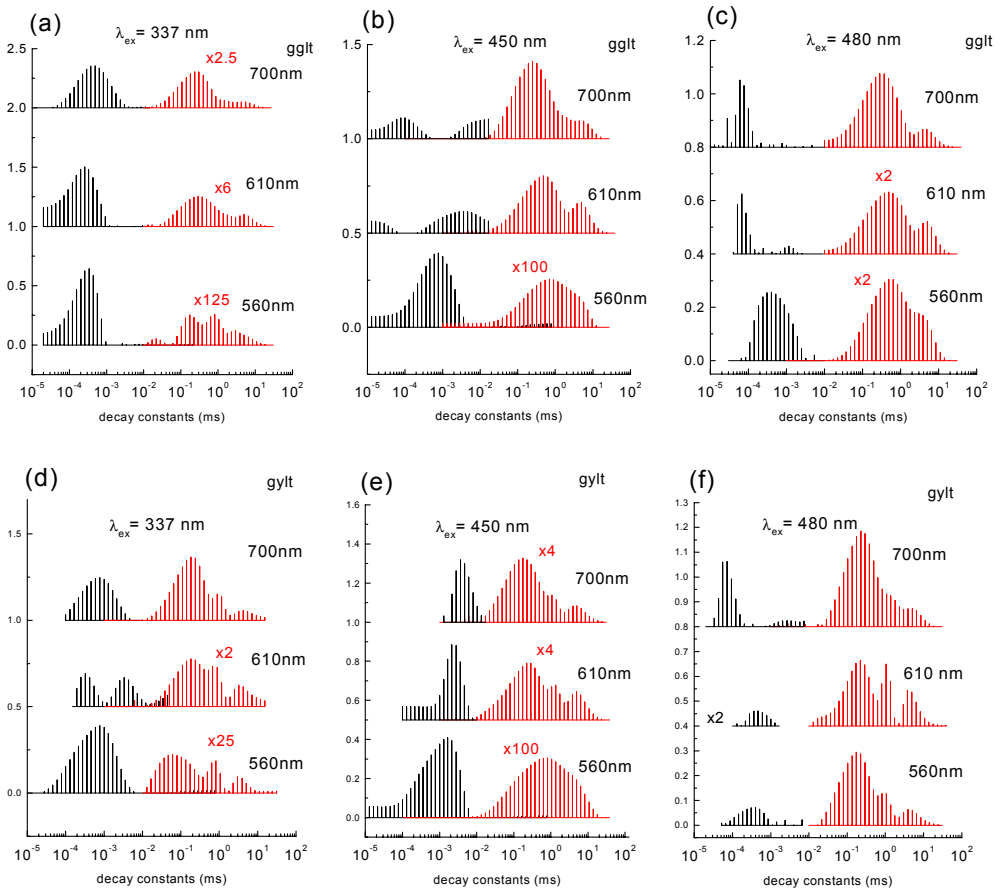

Figure 7. Low temperature emission decay histograms: amplitudes versus decay constants for the green (a)–(c) and yellow (d)–(f) sample.

To perform the calculations we have approximated the continuous decay times distribution by a discrete distribution of the decays constantly spaced on the logarithmic scale as follows:

$$\int A(\tau)\mathrm{e}^{-\frac{t}{\tau}}\,\mathrm{d}(\ln\tau) \approx \sum_i A_i \mathrm{e}^{-t/\tau_i}. \tag{3}$$

Usually good results are obtained when the increase of τ by a factor of 10 is covered by about 10 different time constants.

Typical low temperature decay distributions are illustrated in figures 7 and 8. It is seen that at LT the decays are strongly not single-exponential, having at least a two-peak distribution and depend on the emission as well as excitation wavelengths. At RT the luminescence decay changes qualitatively. The fastest and the slowest decays disappear and the decay becomes practically single-exponential for all excitation and emission wavelengths.

Since at low temperature the luminescence decay times changed over several orders of magnitude the measuring of the long living luminescence tail with the time gate short enough to detect details of the fast component would be rather unreasonable. This is why we recovered the distribution of the time constants of the fast decaying luminescence using the results obtained with the short gate and the distribution of the long living luminescence from separate

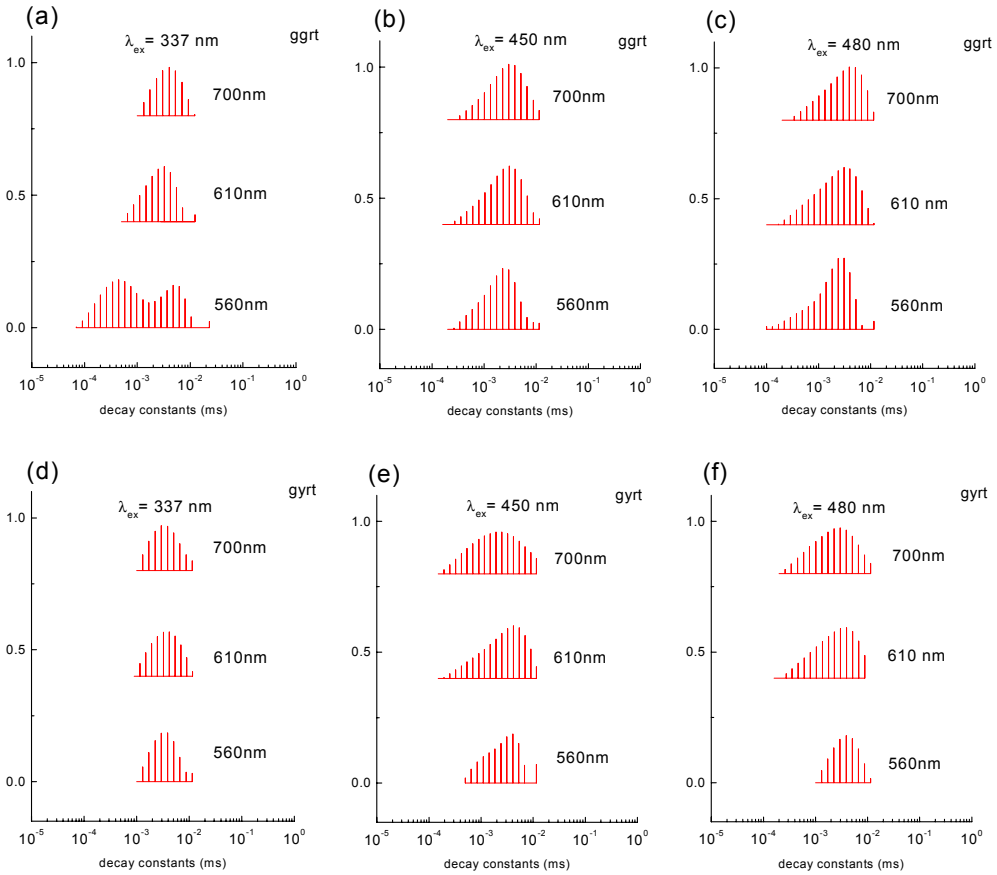

Figure 8. RT emission decay histograms: amplitudes versus decay constants for the green (a)–(c) and yellow (d)–(f) sample.

experiments performed with the much longer gate. Then the recovered distributions have been sewn up and presented as histograms. We repeated such a procedure with different lengths of the time gates and obtained very similar lifetime distributions. Therefore we believe in the reliability of the obtained results.

To recover the time constant distributions we have analysed the decays for two samples: green and yellow. The LT decay time distributions are presented in figures 7(a)–(c) and 7(d)–(f) for the green and yellow samples, respectively.

Under excitation at 337.1 nm the distribution reveals the structure that consists of two groups of decays. The dominant contribution to the emission is given by fast decaying luminescence (decay constants of the order of 0.2–0.3 μs). The longer decaying luminescence seems to be a superposition of the emission from two sites contributing with time constants 200 μs and 4 ms. For the luminescence monitored at 560 nm the short component is of about 120 times greater amplitude than the longer decaying luminescence. The contribution from the longer decaying luminescence increases for longer emission wavelengths, whereas for excitation at 337.1 nm for all the monitored wavelengths the short component is dominating. The situation is similar when the emission monitored at 560 nm is excited at 450 and 480 nm. However, under longer wavelength excitation the short component almost disappears when

the emission is monitored at 610 and 700 nm. In all cases the longer component consists of two decay constants: 200 μs and 5 ms. A weak contribution of the sites with luminescence decay constants of about 10–20 μs is also seen. However, the emission that decays with these times seems to be too weak to be distinguished as a separate peak in the distribution function.

In the case of the yellow sample the distribution of the decay constants and its dependence on the emission and excitation wavelengths is very similar to that of the green sample. The main difference is in the long living luminescence. At low temperature the distribution of the long living luminescence consists of three components peaking at 0.2, 1 and 4 ms. The short decaying luminescence seems to be characterized by a single distribution with the maximum around 1 μs. The cases where the fast decaying luminescence lifetime distribution has the more complex structure (the luminescence monitored at 610 nm with 337.1 nm excitation or monitored at 700 nm with 480 nm excitation) have to be attributed to experimental errors rather than to real physical phenomena. In these cases the contribution from the fast decaying emission is too weak to be recovered with satisfying certainty.

In view of a terrible complication of the presented LT histograms, that are derived from sometimes noisy decay profiles, we can simplify the conclusions drawn from these observations. Hence summarizing one can say that for 337.1 nm excitation the short decays prevail in the overall luminescence which partly holds for the 450 nm excitation (especially for the yellow sample), and for 480 nm excitation a long decay starts to play a substantial part in the luminescence which is also distinct for the yellow sample.

At RT the luminescence decays tend to be almost single-exponential (see figures 8(a)–(f)). Actually the distribution of the decay constants is asymmetrical and extends over an order of magnitude with the maximum at about 3 μs. The evident tail into the shorter time direction is likely related to the contribution of the fast decaying luminescence seen at low temperature. Only emission at 560 nm under 337.2 nm excitation has evidence of two maxima.

One can see that in both samples the fast decaying luminescence is excited quite effectively by 337.1 nm and contributes to the emission spectrum mainly in the short wavelength region, whereas the slowly decaying luminescence is easily excited by 450 and 480 nm and contributes to the spectrum in the long wavelength region.

5.2. Interpretation

Different time constants of the emission should be related to the specific centres. As shown in the analysis of the luminescence excitation and absorption spectra there are at least two kinds of ions active in both samples, namely Cr^{5+} and Cr^{6+}. The octahedrally coordinated Cr^{5+} is the $3d^1$ system where the optical transitions, parity forbidden and spin allowed, take place between the $^2T_{2g}$ ground and the ^2E_g excited electronic manifolds. The system is thus equivalent to the well known Ti^{3+}. By comparison with the Ti^{3+} one expects lifetimes of the order of a few microseconds. This prediction fits well with the 3–4 μs decay constants detected for all the samples at RT. At low temperature the longer components appear in the vicinity of tens μs, spreading up to milliseconds.

It is evident that the short decay emission is effectively excited by 337.1 nm wavelength. The absorption and excitation spectra suggest that this emission can be related to the excitation of the $Cr^{6+}O^{2-}$ centre. The $Cr^{5+}O^{-}$ centre which forms after the CT transitions via the GSA in the frame of the $[CrO_4]^{2-}$ group has the triplet and singlet excited terms whereas the ground state is a fully symmetrical singlet term. It is believed [26] that the $[CrO_4]^{2-}$ group rather does not produce any luminescence, although the triplet–singlet (T–S) transitions are quite common in such a centre type [27, 28]. Indeed, in our previous paper [11] we demonstrated such a lack of $[CrO_4]^{2-}$ luminescence in the LBO:Cr glass. The existence or lack of such

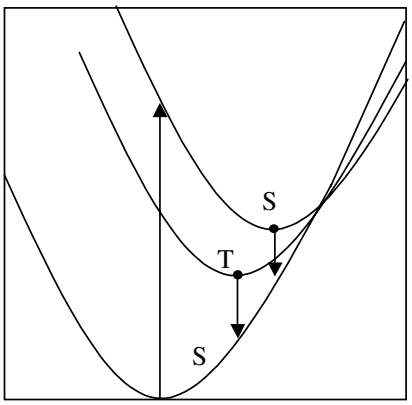

Figure 9. Qualitative illustration of the singlets and triplets of the $3d^1 2p^5(t_1^5, 2e)$ configuration showing how the shorter singlet decay can be associated with wavelengths longer than that of triplet.

a TS luminescence is determined by the strength of the electron–lattice coupling of the first excited triplet state with respect to the singlet ground state. Thus we have two factors that are detrimental: the spin selection rule and a relatively large electron–lattice coupling which allows for effective radiationless transitions. However, there are still the excited singlets, which could yield the luminescence in a specific situation. First, the transitions from them are spin-allowed; hence even strong electron–lattice coupling is not able to entirely quench the luminescence via radiationless transitions. Instead it can at most shorten the singlet–singlet (S–S) luminescence lifetime. This would be a 'hot luminescence', spin and parity allowed fast transition. It should be seen at LT rather than RT because RT would kill the luminescence via radiationless transitions. The situation, which by the way can also explain the faster decay of the longer wavelength component of the emission spectrum, is schematically illustrated in figure 9.

In this context there is another interesting observation: going back to figure 5 we can now comment on a very interesting decay profile detected at $\lambda_{obs} = 560$ nm. There is a domination of short decay, which seems to be in contradiction with the previous observations that transitions at longer wavelengths are responsible for shorter times (see TRE spectra). However careful inspection of figure 2 shows that such a contradiction does not take place. Monitoring the LT decay at $\lambda_{obs} = 560$ nm we deal with the photon energy 17 860 cm^{-1}. Looking at the Gaussian components of the overall spectrum one can see that at 17 860 cm^{-1} only one component remains—the one which peaks at $\sim$13 000 cm^{-1} and is ascribed to the $Cr^{5+}O^{-}$ centre. At LT this luminescence is dominated by the S–S transitions and hence the domination of short decay at 560 nm.

It is characteristic that at RT we observe a multiexponential decay of the time constant distribution centred around a rather short time ($\sim\mu$s); the long component disappears.

Usually spin forbidden but symmetry allowed transitions yield the luminescence of a decay constant falling in the several microseconds region (e.g. [29, 30]). This, of course, depends on several other factors, of which the probability of the nonradiative transitions is the most important one. Here we deal with milliseconds at LT which at RT transforms to microseconds. This can suggest the importance of the nonradiative transitions. On the other hand, in this type of material an existence of metastable trap states (e.g. thermoluminescent traps) has been reported at least several times (e.g. [8, 31]). They could play a role in the long component seen at LT since we observed at least two or even three different decay constants looking

like being related to one site. Such an effect is possible only when one assumes metastable traps of different depths that can accumulate the excitation energy from the centre. Thus the luminescence decay can be controlled by the trap-centre nonradiative transition rate [32, 33]. Hence at this stage we can state as follows: the long component seen at LT can be ascribed to the $[CrO_4]^{2-}$ group {triplets of $Cr^{5+}O^-$ ($3d^12p^5$) (t_1^5, 2e) configuration} and/or to the $Cr^{5+}(O_h)$ ions with an influence of some metastable traps.

For a better insight into the problem of traps we have performed thermoluminescence measurements, obtaining as results the glow curves peaking at ∼125, ∼225, ∼470 and ∼600 K, i.e. the thermoluminescent traps could lengthen the luminescence decay at temperatures at least as low as those mentioned. Hence none of them could give a contribution to the long component seen at 10 K. Therefore we can only resort to the first option, i.e. to the very low rate of nonradiative transitions between triplets of ($3d^12p^5$) configuration of the $Cr^{5+}O^-$ centre and ground state singlet of ($3d^02p^6$) configuration of the Cr^{6+} centre. In the case of a very high barrier between these states and a very low temperature the millisecond decay times seem to be likely. The results of the ESA measurements appeared to support this hypothesis.

6. EPR measurements

To make sure that, apart from the $[CrO_4]^{2-}$ group (Cr^{6+} ions) we deal also with the Cr^{5+} ions of six-fold coordination, we have performed EPR measurements. The EPR spectra were detected at RT using a Bruker B-ER-418SM spectrometer. The microwave frequency was determined with the use of a Marconi Instruments frequency meter (18 GHz microwave counter 2440) with a precision of 1 kHz. The two Cr-doped silica sol–gel glass samples showed similar double EPR lines for both. The typical resulting spectra are presented in figures 10(a), (b) for green and yellow samples, respectively. In table 1 the magnetic induction values for characteristic positions A, a, b of registered lines as well as the corresponding g factors are specified. The values of peak-to-peak widths ΔB_{pp} and the distances of maxima ($B_a - B_A$) are also presented. The most important features of the spectrum are the double-line character and relatively small linewidths (in comparison to that of Cr^{3+} ions sometimes occurring in other glasses). Because in our sol–gel glass there is practically no trace of Cr^{3+} ions (otherwise they would be seen in the optical spectra) both mentioned features can be connected with the existence of the Cr^{5+} ions in the octahedral coordination. Typical EPR spectra for Cr^{3+} ions show ΔB_{pp} of some hundred G that are usually associated with the ion–ion interactions [34]. A very low background of this type is also observed in our measurements. ΔB_{pp} for Cr^{5+}, however, are always smaller than 40 G [35]. As is seen in our samples ΔB_{pp} is of about 20 G. This indicates that in the measured samples the chromium activator occurs in the form of a pentavalent ion. The next consideration is the double-line structure. Because the g factor should be insensitive to the magnetic field direction (the directional distribution of the Cr^{5+} sites in glass is quite isotropic) the double-line structure suggests that the Cr^{5+} ions are situated in two different positions. As shown in [36] such a structure is typical for the six-fold-coordinated Cr^{5+} ions where a number of them resides in tetragonally distorted sites, i.e. where the Cr^{5+} ion is displaced from the centre of the octahedron along one of the cubic axes. The tetragonal distortion, being a deviation from the full symmetry, is then connected with a relaxation of the orbital degeneration in the ground state [22, 36]. This is equivalent to the mentioned JT effect and additionally supports the described double structure seen in the LT luminescence spectrum. In this context a different balance of the two EPR peaks for our samples can be interpreted as a different extent of the tetragonal distortions.

Such a situation leads, of course, to the appearance of two lines with different g factors, as seen in table 1. Moreover, sample 2 (green) shows a lower intensity of the EPR signal

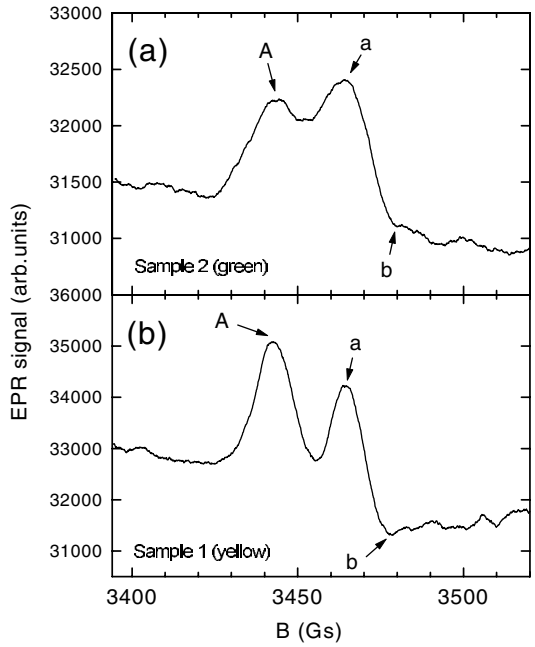

Figure 10. EPR spectra for green (a) and yellow (b) sample.

Table 1. Parameters derived from the EPR measurements.

Samples	B_A	B_a	B_b	ΔB_{pp}^{ab}	g_A	g_a	I_a
1 (yellow)	3442.170	3464.546	3478.249	13.703	1.984 90	1.972 03	525.4
2 (green)	3443.480	3463.554	3478.279	14.725	1.982 47	1.970 98	241.4

than sample 1 (yellow) although the chromium concentration in both is similar and even a bit larger in the green sample. This can be explained by a different balance of the Cr^{5+}/Cr^{6+} concentrations in the samples, suggesting that in the green sample, as a result of a little different preparation conditions, more chromium ions reach a higher oxidation state and end up in a Cr^{6+} nonparamagnetic form. Luminescence investigations seem to confirm this hypothesis.

7. Excited state absorption

The ESA spectrum, measured with the 308 nm excitation, is presented in figure 11. The spectrum is expressed in terms of the absorption coefficient α_{ESA} and is free from the influence of the GSA bleaching [5, 16] for the excitation ratios N^*/N_0 smaller than 0.01, which is well satisfied in our experiment. The double-band ESA spectrum suggests an existence of two well defined states, terminal for the ESA transitions. We have attempted to fit those two bands by two Gaussians on the energy scale.

According to interpretation of the ESA spectrum, we should first of all note that from the simplest theoretical point of view there is no reason for any ESA to exist from the ^2E_g state of the $Cr^{5+}(O_h)$ ions to some higher lying states of these ions because they simply do not exist since the Cr^{5+} is a typical d^1 system with only one excited term, ^2E_g (not counting the JT or lower symmetry splittings). However, there is still a possibility for the ESA transitions from

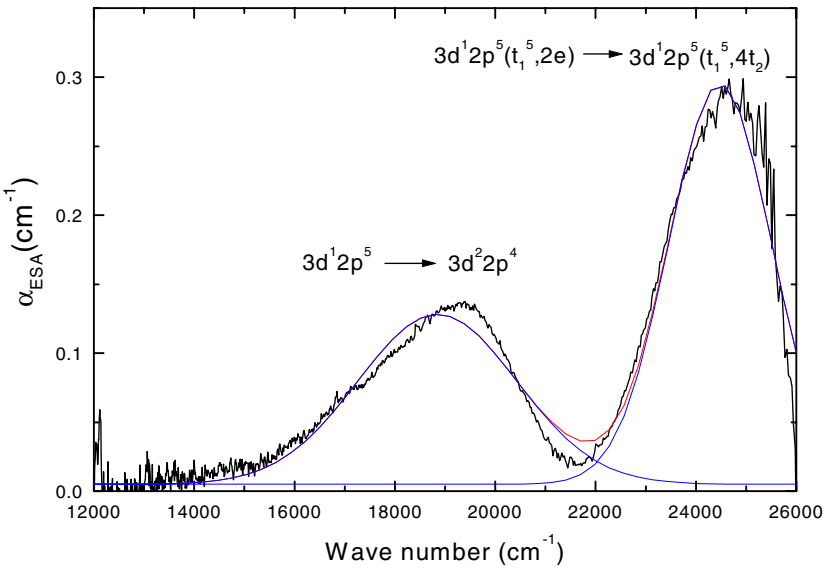

Figure 11. ESA spectrum for 308 nm excitation. Thin smooth lines are Gaussian fits.

this term to the states forming the conduction band of the glass phase or to possible CT states in the frame of the $[CrO_6]^{7-}$ group and, finally, as mentioned in section 3, to the CT states in the frame of the $[CrO_4]^{4-}$ group. The absorption and excitation spectra prove that the bottom of the conduction band lies relatively close to the ^2E_g state, hence the possible ESA spectrum, if it exists, will be rather broad, structureless and positioned in the infrared range. We observe, however, the distinct spectrum of two well defined bands and, in view of this, we can recall our last results obtained for the $Li_2B_4O_7$ glass activated by chromium [11] where a very similar situation occurred.

According to the latter two options, i.e. possible ESA transitions to the CT states of the $Cr^{5+}(O_h)$ ions or transitions to the CT states of the $Cr^{4+}(T_d)$ ions, we can only state that in the range of the experiment we do not observe any distinct features in the absorption and luminescence excitation that could be connected with the CT in the $Cr^{5+}(O_h)$ ions, and for $Cr^{4+}(T_d)$ ions, in [11] we have observed and interpreted quite similar ESA spectra in the material with no trace of Cr^{4+} ions.

Summarizing our points concerning the double-band ESA seen in [11] and in the present work we can state as follows: the only centre responsible for the observed ESA spectrum is $Cr^{5+}O^-$ which forms via the CT transition in the frame of the $[CrO_4]^{2-}$ group. The $Cr^{6+}O^{2-}$ centre is a typical example of the d^0 complex of approximately tetrahedral coordination where the highest filled molecular orbital of the ground state is made mostly of ligand 2p orbitals of the $t_1\pi$ symmetry [37]. The GSA transition corresponds, simplifying, to the transition of one of the electrons taking part in oxygen bonds to the free d^0 orbital of the central ion, leaving a hole in the bonds. This is the CT transition mentioned[3]. Thus the excited centre, $Cr^{5+}O^-$, creates and in the crystal field its five-fold degenerated $3d^12p^5$ electronic configuration splits into a two-fold degenerated state of the 2e symmetry and a three-fold degenerated state of the $4t_2$ symmetry. In the crystal field approximation both these states are distanced by the $10Dq$

[3] There are several papers treating the CT transitions rather as the redistribution of orbitals [38] and/or transitions of a rather small part of the charge [39]. However, the simple CT model is still successful in describing the optical properties of the system [11, 28, 30], whether the transfer concerns 100% or several per cent of the charge.

Table 2. Parameters used to create the SCC diagram explaining the ESA spectrum shown in figure 11.

Parameter	κ	$\hbar\omega$	$\hbar\omega'$	kT	CT_1	CT_2	Γ_1	Γ_2	Γ_3	ESA_1	ESA_2
Energy (cm^{-1})	8000	250	200	200	27 029	46 200	3229	3171	2036	18 846	24 481

energy. The transitions between terms of this configuration, $3d^12p^5(t_1^5, 2e) \rightarrow 3d^12p^5\ (t_1^5, 4t_2)$, are responsible for the higher (and narrower) ESA band. A second ESA band can be ascribed to the transitions between $3d^12p^5(t_1^5, 2e)$ and a term of different configuration, $3d^22p^4$, which can form after two consecutive transfers of electrons from ligands to the central ion. Such a state, having a substantially different charge distribution, will be more strongly coupled to the lattice and will be characterized by a different phonon energy. The relatively high strength of the ESA can be consistent with the familiar theoretical fact that for the T_d symmetry the transitions should be of much higher probability than those for the O_h symmetry because of a lack of inversion symmetry in T_d.

Using the Gaussians that fit the experimental ESA spectrum and parameters taken from the experiment we have attempted to construct a simple single configuration coordinate (SCC) diagram, which can explain the double-band ESA spectrum. Apart from a single coordinate we have assumed a harmonic approximation and linear coupling to the lattice, at least for the states of $3d^02p^6$ and $3d^12p^5$ configuration. We have used the following experimental data: CT_1 is the energy of the first CT peak in the absorption spectrum; $\Gamma_{1,2,3}$ are the bandwidths at half maximum (FWHM), respectively, of the CT_1 band, lower energy ESA band and higher energy ESA band; and $ESA_{1,2}$ are the peak positions (on the energy scale) of the lower and higher energy ESA bands, respectively. The definitions and equations leading to the unambiguous determination of the SCC diagram were given in [11]. For our purposes we can add definitions of three other parameters: κ—the elastic constant describing the parabolas curvature and $\hbar\omega$—the phonon energy of the ground, first (2e) and second ($4t_2$) excited state, and $\hbar\omega'$—the same for the $3d^22p^4$ state. The parameter CT_2 plays the role of the fitting parameter [11].

Table 2 shows the parameters taken to create the SCC diagram as presented in figure 12. The right-hand side of figure 12 shows the Gaussians fitting the experimental ESA spectrum (figure 11). One can note that in figure 12 the Gaussian fit is not ideal (it is seen especially for the lower and broader ESA_1 band). We choose the Gaussians for simplicity: the actual asymmetrical shape of the ESA_1 band can be explained by the influence of the possible JT effect of similar type as described in [40].

It is perhaps worthwhile noting that the presented SCC diagram is a great simplification, which only provides an idea of how the double-band ESA can occur in the frame of the $[CrO_4]^{2-}$ group. However, it can explain a fundamental observation that the $[CrO_4]^{2-}$ group sometimes (like in the LBO glass [11]) does not give rise to the luminescence and sometimes does (like in our sol–gel glass). The most important difference between these two systems is the energy barrier between the $3d^12p^5$, $(t_1^5, 2e)$ excited state and $3d^02p^6$, (t_1^6) ground state. The lower barrier for the LBO glass and the much higher one for the sol–gel glasses can explain the lack of $[CrO_4]^{2-}$-related luminescence in the former (because of the radiationless transitions) and the presence of such a luminescence in the latter.

8. Discussion and conclusions

As we could see, the optical properties of the Cr:silica sol–gel glass are associated with two types of centres: six-fold-coordinated Cr^{5+} ions and four-fold-coordinated Cr^{6+} ions, the latter

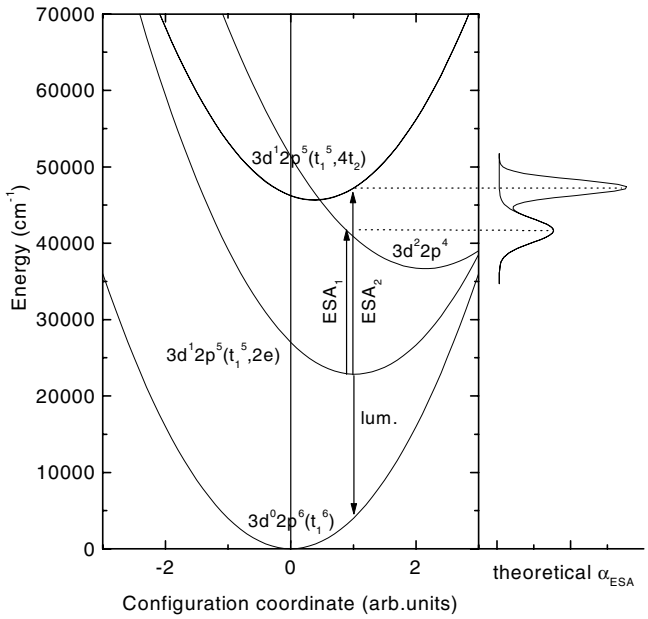

Figure 12. SCC diagram explaining the ESA spectrum. The right-hand side shows the Gaussians fitting the experimental ESA spectrum from figure 11.

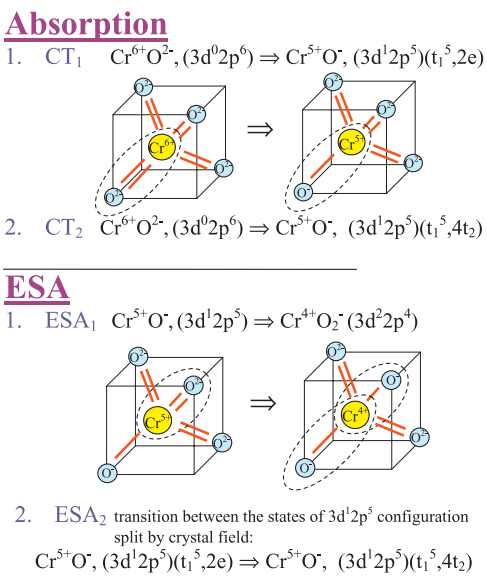

Figure 13. Ball and stick model illustrating the ground and ESA in the frame of the $[CrO_4]^{2-}$ group.

occurring in the frame of the $[CrO_4]^{2-}$ group. The Cr^{5+} ions are usually believed to occur in the four-fold coordination of $\sim T_d$ symmetry [8, 41, 42]. However, as mentioned in [8] the loose structure of the glass and corresponding ionic radii makes equally possible the occurrence of the Cr^{5+} ions in ∼tetrahedral as well as in ∼octahedral coordination. We believe that, unlike

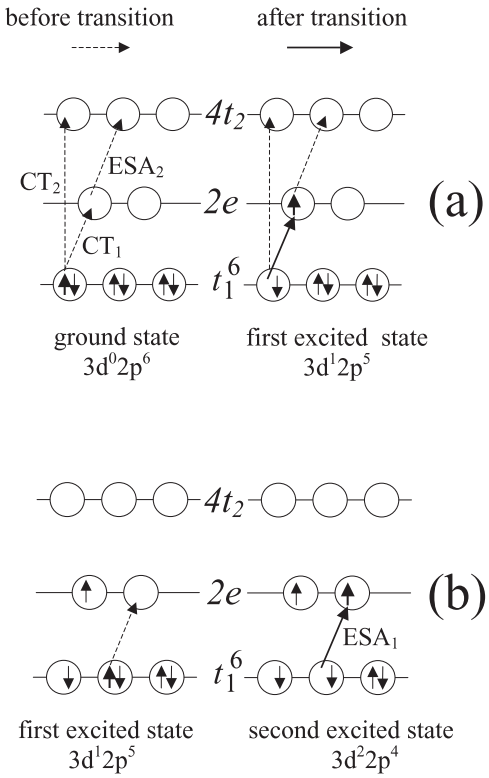

Figure 14. Single-electron model explaining the GSA and ESA transitions in terms of molecular-orbital energy levels in the tetra–oxo complexes, (a) GSA(CT_1), GSA(CT_2) and ESA_2 transitions, (b) ESA_1 transition (see figure 12).

in [8], in our sol–gel samples the Cr^{5+} ions occur in the ∼octahedral coordination. Apart from our EPR results and described JT effect with all the nuances typical for O_h symmetry, this can be proved by the following simple consideration: in the case of the d^1 system the ^2E_g state is distanced from the $^2T_{2g}$ state by an energy $10Dq$ being the measure of the crystal field. Since transitions between these states correspond to the $10Dq$ energy the positions of the emission band will be correlated with the fact if the Cr^{5+} ions occupy tetrahedral (T_d) or octahedral (O_h) sites. Taking the familiar relation (e.g. [43]):

$$10Dq(O_h) = -\tfrac{9}{4}10Dq(T_d) \tag{4}$$

and assuming the same strength of electron–lattice coupling for both types of sites, we can see that the energy of the emission spectrum maximum reported for Cr^{5+} (T_d) in [8] (6667 cm^{-1}, 1.5 μm) translates, according to (4), to the energy 15 000 cm^{-1} (667 nm) which falls exactly into the energy of the observed component of the emission spectrum ascribed to $Cr^{5+}(O_h)$ in this work (see figure 2). Other arguments for such an ascription are: the occurrence of a very characteristic behaviour typical for the JT effect in the $d^1(O_h)$ systems, described in section 4, and our EPR results.

For the remaining part of the optical properties of the described material are responsible for the transitions in the frame of the $[CrO_4]^{2-}$ group. Figure 13 illustrates a simple ball and stick model of the CT GSA ($CT_{1,2}$) and the ESA_1, ESA to the terminal double-electron state $3d^22p^4$. It is seen that the hole in the bonds after a CT_1 or CT_2 transition introduces an asymmetry in the

complex, which could lead to the coupling to different vibrational modes than in the ground state. The ESA_1 transition causes the next modification of the complex ($Cr^{4+}O^{2-}$ centre) which now, having two holes in the bonds, should be even further from the fully symmetrical vibration mode than the $Cr^{5+}O^{-}$ centre. Such couplings to the lower symmetry modes are the bases of the JT effect. Thus we can say that not only in the six-fold-coordinated Cr^{5+} centre does the JT effect occur, but also in the four-fold-coordinated Cr^{6+} centre. Moreover, the deeper insight into this mechanism suggests that the transition, $Cr^{6+}O^{2-} \rightarrow Cr^{5+}O^{-}$, can be associated with the coupling to the three-dimensional mode τ whereas the transition, $Cr^{6+}O^{2-} \rightarrow Cr^{4+}O^{2-}$ or $Cr^{5+}O^{-} \rightarrow Cr^{4+}O^{2-}$, can be associated with the coupling to the two-dimensional mode ϵ. This type of JT effect can explain the asymmetry of the ESA (especially the ESA_1) bands [40].

On the other hand, the above model, explaining the double-band ESA in the frame of the $[CrO_4]^{2-}$ group, can be expressed in terms of the single-electron transition between the molecular-orbital energy levels characteristic for the tetra–oxo complexes [28, 37]. It is seen in figures 14(a), (b) presenting the simplified description of the situation before and after the transitions.

Acknowledgments

This work was supported by the State Committee for Scientific Research (KBN) under grant number 2 P03B 117 16 and by the Rector of the Nicholas Copernicus University in Toruń, who made possible the visit to the University of Strathclyde, Glasgow, for the collaborative work. We are very grateful to Dr T P Han of the University of Strathclyde, Glasgow, UK, for rendering assistance in the measurements performed at the Department of Physics and Applied Physics, and to Professor W Stręk of the Institute of Low Temperature and Structure Research, Polish Academy of Sciences, Wrocław, Poland, for supplying the samples and fruitful discussions. We are indebted to M Ptaszyk of our Institute for his assistance in elaborating the EPR data. One of the authors (MG) was also supported by the Gdaúsk University under grant number: 5200-5-0312-2.

References

[1] van Die A, Blasse G and van der Weg W F 1985 *J. Phys. C: Solid State Phys.* **18** 3379
[2] Rasheed F, O'Donnell K P, Henderson B and Hollis D B 1991 *J. Phys.: Condens. Matter* **3** 3825
[3] Hömmerich U, Eilers H, Yen W M, Hayden J S and Aston M K 1994 *J. Lumin.* **60/61** 119
[4] Murata T, Torisaka M, Takebe H and Morinaga K 1997 *J. Non-Cryst. Solids* **220** 139
[5] Stręk W, Łukowiak E, Dereń P J, Maruszewski K, Trabjerg I, Koepke Cz, Malashkevich G E and Gaishun V I 1997 *Proc. SPIE* **3176** 249
[6] Herren M, Nishiuchi H and Morita M 1994 *J. Chem. Phys.* **101** 4461
[7] Morita M, Miyazaki N, Murakami S, Herren M and Rau D 1998 *J. Lumin.* **76/77** 238
[8] Stręk W, Dereń P J, Łukowiak E, Hanuza J, Drulis H, Bednarkiewicz A and Gaishun V 2001 *J. Non-Cryst. Solids* **288** 56
[9] Wegner T and Petermann K 1989 *Appl. Phys.* B **49** 275
[10] Yuan H, Jia W, Cohen D, Yen W M and Aitken B G 1997 *Mater. Res. Soc. Symp. Proc.* **455** 483
[11] Koepke Cz, Wisniewski K, Grinberg M, Majchrowski A and Han T P J 2001 *J. Phys.: Condens. Matter* **13** 2701
[12] Hazenkamp M F, Güdel H U, Atanasov M, Kesper U and Reinen D 1996 *Phys. Rev.* B **53** 2367
[13] Wissing K, Barriuso M T, Aramburu J A and Moreno M 1999 *J. Chem. Phys.* **111** 10217
[14] Grinberg M, Russell D L, Holliday K, Wisniewski K and Koepke Cz 1998 *Opt. Commun.* **156** 409
[15] Koepke Cz, Wisniewski K, Grinberg M, Russell D L and Holliday K 1999 *J. Lumin.* **81** 301
[16] Koepke Cz, Wisniewski K, Grinberg M, Russell D L, Holliday K and Beall G H 1998 *J. Lumin.* **78** 135
[17] Powell R C 1998 *Physics of Solid-State Laser Materials* (New York: American Institute of Physics)
[18] Koechner W 1996 *Solid-State Laser Engineering* (Berlin: Springer)
[19] Yamaga M, Gao Y, Rasheed F, O'Donnell K P, Henderson B and Cockayne B 1990 *Appl. Phys.* B **51** 329

[20] Meyn J-P, Danger T, Petermann K and Huber G 1993 *J. Lumin.* **55** 55
[21] Herzberg G 1966 *Molecular Spectra and Molecular Structure, III. Electronic Spectra and Electronic Structure of Polyatomic Molecules* (New York: Van Nostrand-Reinhold)
[22] Sturge M D 1967 The Jahn–Teller effect in solids *Solid State Physics, Advances in Research and Applications* ed F Seitz, D Turnbull and H Ehrenreich (New York: Academic) pp 91–211
[23] Wang G, Gallager H G, Han T P J, Henderson B, Yamaga M and Yosida T 1997 *J. Phys.: Condens. Matter* **9** 1649
[24] Macfarlane R M, Wong J Y and Sturge M D 1968 *Phys. Rev.* **166** 250
[25] Albers P, Stark E and Huber G 1986 *J. Opt. Soc. Am.* B **3** 134
[26] Blasse G 1980 The luminescence of closed-shell transition-metal complexes. New developments *Luminescence and Energy Transfer, Structure and Bonding* vol 42 (New York: Springer) p 1
[27] Grasser R and Scharmann A 1976 *J. Lumin.* **12/13** 473
[28] Koepke Cz, Wojtowicz A J and Lempicki A 1995 *IEEE J. Quantum Electron.* **31** 1554
[29] Koepke Cz and Lempicki A 1991 *J. Lumin.* **47** 189
[30] Koepke Cz, Wojtowicz A J and Lempicki A 1993 *J. Lumin.* **54** 345
[31] Del Nery S M, Pontuschka W M, Isotani S and Rouse C G 1994 *Phys. Rev.* B **49** 3760
[32] Wojtowicz A J, Glodo J, Drozdowski W and Przegietka K R 1998 *J. Lumin.* **79** 275
[33] Wojtowicz A J, Glodo J, Lempicki A and Brecher C 1998 *J. Phys.: Condens. Matter* **10** 8401
[34] Łodzińska A, Polakiewicz M, Rozpłoch F and Kachniarz E 1992 *Polish J. Chem.* **65** 1481
[35] O'Reilly D E and McIver D S 1960 *Adv. Catal.* **12** 100
[36] Lagendijk A, Morel R J, Glasbeek M and van Voorst J D W 1972 *Chem. Phys. Lett.* **12** 518
[37] Ballhausen C J and Gray H B 1964 *Molecular Orbital Theory* (New York: Benjamin) pp 123–8
[38] Ziegler T, Rauk A and Baerends E J 1976 *Chem. Phys.* **16** 209
[39] Stückl A C, Daul C A and Güdel H U 1997 *J. Chem. Phys.* **107** 4606
[40] Grinberg M, Kaczmarek S M, Berkowski M and Tsuboi T 2001 *J. Phys.: Condens. Matter* **13** 743
[41] Gaft M, Boulon G, Panczer G, Guyot Y, Reisfeld R, Votyakov S and Bulka G 2000 *J. Lumin.* **87/89** 1118
[42] Ishii T, Ogasawara K, Adachi H and Tanaka I 2001 *Appl. Phys. Lett.* **78** 2154
[43] Henderson B and Imbusch G F 1989 *Optical Spectroscopy of Inorganic Solids* (Oxford: Clarendon)